7. S. M. Bachilo *et al.*, *J. Am. Chem. Soc.* **125**, 11186 (2003).
8. Y. M. Li *et al.*, *Nano Lett.* **4**, 317 (2004).
9. P. Collins, M. Arnold, P. Avouris, *Science* **292**, 706 (2001).
10. R. Seidel *et al.*, *Nano Lett.* **4**, 831 (2004).
11. D. Chattopadhyay, L. Galeska, F. Papadimitrakopoulos, *J. Am. Chem. Soc.* **125**, 3370 (2003).
12. M. Zheng *et al.*, *Science* **302**, 1545 (2003).
13. M. S. Strano *et al.*, *Science* **301**, 1519 (2003).
14. K. Balasubramanian, R. Sordan, M. Burghard, K. A. Kern, *Nano Lett.* **4**, 827 (2004).
15. L. An, Q. A. Fu, C. G. Lu, J. Liu, *J. Am. Chem. Soc.* **126**, 10520 (2004).
16. W. Kim *et al.*, *Appl. Phys. Lett.* **87**, 1 (2005).
17. J. Kong, H. Soh, A. Cassell, C. F. Quate, H. Dai, *Nature* **395**, 878 (1998).
18. Materials and methods are available as supporting materials on *Science* Online.
19. G. Y. Zhang *et al.*, *J. Am. Chem. Soc.* **128**, 6026 (2006).
20. G. Drabner, A. Poppe, H. Budzikiewicz, *Int. J. Mass Spectrom. Ion Process.* **97**, 1 (1990).
21. W. Zhou *et al.*, *Chem. Phys. Lett.* **350**, 6 (2001).
22. Y. Li *et al.*, *J. Phys. Chem. B* **109**, 6968 (2005).
23. H. Park, J. Zhao, J. P. Lu, *Nanotechnology* **16**, 635 (2005).
24. T. Heitz, B. Drevillon, C. Godet, J. E. Bouree, *Phys. Rev. B* **58**, 13957 (1998).
25. J. Guo, S. Goasguen, M. Lundstrom, S. Datta, *Appl. Phys. Lett.* **81**, 1486 (2002).

26. We thank Intel and MARCO Center for Materials, Structures, and Devices for support of this work.

Supporting Online Material
www.sciencemag.org/cgi/content/full/314/5801/974/DC1
Materials and Methods
Figs. S1 to S3

11 August 2006; accepted 3 October 2006
10.1126/science.1133781

Metamaterial Electromagnetic Cloak at Microwave Frequencies

D. Schurig,[1] J. J. Mock,[1] B. J. Justice,[1] S. A. Cummer,[1] J. B. Pendry,[2] A. F. Starr,[3] D. R. Smith[1]*

A recently published theory has suggested that a cloak of invisibility is in principle possible, at least over a narrow frequency band. We describe here the first practical realization of such a cloak; in our demonstration, a copper cylinder was "hidden" inside a cloak constructed according to the previous theoretical prescription. The cloak was constructed with the use of artificially structured metamaterials, designed for operation over a band of microwave frequencies. The cloak decreased scattering from the hidden object while at the same time reducing its shadow, so that the cloak and object combined began to resemble empty space.

A new approach to the design of electromagnetic structures has recently been proposed, in which the paths of electromagnetic waves are controlled within a material by introducing a prescribed spatial variation in the constitutive parameters (*1*, *2*). The recipe for determining this variation, based on coordinate transformations (*3*), enables us to arrive at structures that would be otherwise difficult to conceive, opening up the new field of transformation optics (*4*, *5*).

One possible application of transformation optics and media is that of electromagnetic cloaking, in which a material is used to render a volume effectively invisible to incident radiation. The design process for the cloak involves a coordinate transformation that squeezes space from a volume into a shell surrounding the concealment volume. Maxwell's equations are form-invariant to coordinate transformations, so that only the components of the permittivity tensor ε and the permeability tensor μ are affected by the transformation (*5*), becoming both spatially varying and anisotropic. By implementing these complex material properties, the concealed volume plus the cloak appear to have the properties of free space when viewed externally. The cloak thus neither scatters waves nor imparts a shadow in the transmitted field, either of which would enable the cloak to be detected. Other approaches to invisibility either rely on the reduction of backscatter or make use of a resonance in which the properties of the cloaked object and the cloak itself must be carefully matched (*6*, *7*).

It might be of concern that we are able to achieve two different solutions to Maxwell's equations that both have, in principle, the exact same field distributions on a surface enclosing the region of interest. Indeed, the uniqueness theorem would suggest that these two solutions would be required to have the exact same medium within the surface. The uniqueness theorem, however, applies only to isotropic media (*8*, *9*); the required media that result from our coordinate transformations are generally anisotropic. Such media have been shown to support sets of distinct solutions having identical boundary conditions (*10*, *11*).

The effectiveness of a transformation-based cloak design was first confirmed computationally in the geometric optic limit (*1*, *5*) and then in full-wave finite-element simulations (*12*). Advances in the development of metamaterials (*13*), especially with respect to gradient index lenses (*14*, *15*), have made the physical realization of the specified complex material properties feasible. We implemented a two-dimensional (2D) cloak because its fabrication and measurement requirements were simpler than those of a 3D cloak. Recently, we have demonstrated the capability of obtaining detailed spatial maps of the amplitude and phase of the electric field distribution internal to 2D negative-index metamaterial samples at microwave frequencies (*16*). Using this measurement technique, we confirmed the performance of our cloak by comparing our measured field maps to simulations.

In both the cloaking simulations and the measurements presented here, the object being cloaked is a conducting cylinder at the inner radius of the cloak; this is the largest and most strongly scattering object that can be concealed in a cloak of cylindrical geometry.

For the cloak design, we start with a coordinate transformation that compresses space from the cylindrical region $0 < r < b$ into the annular region $a < r' < b$, where r and r' are the radial coordinates in the original and transformed system, respectively, a is the cloak inner radius, and b is the cloak outer radius. A simple transformation that accomplishes this goal is

$$r' = \frac{b-a}{b} r + a \quad \theta' = \theta \quad z' = z \qquad (1)$$

where θ and z are the angular and vertical coordinates in the original system, and θ' and z' are the angular and vertical coordinates in the transformed system. This transformation leads to the following expression for the permittivity and permeability tensor components

$$\varepsilon_r = \mu_r = \frac{r-a}{r} \quad \varepsilon_\theta = \mu_\theta = \frac{r}{r-a}$$

$$\varepsilon_z = \mu_z = \left(\frac{b}{b-a}\right)^2 \frac{r-a}{r} \qquad (2)$$

Equation 2 shows that all of the tensor components have gradients as a function of radius, implying a very complicated metamaterial design. However, because of the nature of the experimental apparatus, in which the electric field is polarized along the z axis (cylinder axis), we benefit from a substantial simplification in that only ε_z, μ_r, and μ_θ are relevant. Moreover, if we wish to primarily demonstrate the wave trajectory inside the cloak, which is solely determined by the dispersion relation, we gain even more flexibility in choosing the functional forms for the electromagnetic ma-

[1]Department of Electrical and Computer Engineering, Duke University, Box 90291, Durham, NC 27708, USA. [2]Department of Physics, The Blackett Laboratory, Imperial College, London SW7 2AZ, UK. [3]SensorMetrix, 5695 Pacific Center Boulevard, San Diego, CA 92121, USA.

*To whom correspondence should be addressed. E-mail: drsmith@ee.duke.edu

terial parameters. In particular, the following material properties

$$\varepsilon_z = \left(\frac{b}{b-a}\right)^2 \quad \mu_r = \left(\frac{r-a}{r}\right)^2 \quad \mu_\theta = 1 \quad (3)$$

have the same dispersion as those of Eq. 2, implying that waves will have the same dynamics in the medium. In the geometric limit, for example, rays will follow the same paths in media defined by Eqs. 2 or 3, and refraction angles into or out of the media will also be the same (*12*). The only penalty for using the reduced set of material properties (Eq. 3) is a nonzero reflectance.

To implement the material specification in Eq. 3 with a metamaterial, we must choose the overall dimensions, design the appropriate unit cells, and specify their layout, which for our implementation represents a pattern that is neither cubic nor even periodic. All three of these design elements share parameters, making it advantageous and necessary to optimize them all at once. Equation 3 shows that the desired cloak will have constant ε_z and μ_θ, with μ_r varying radially throughout the structure. This parameter set can be achieved in a metamaterial in which split-ring resonators (SRRs), known to provide a magnetic response that can be tailored (*17*), are positioned with their axes along the radial direction (Fig. 1).

As can be seen from Eq. 3, the transformed material properties depend strongly on the choice of a and b . Because of constraints from the unit cell design and layout requirements, we chose the seemingly arbitrary values a = 27.1 mm and b = 58.9 mm. The resulting material properties are plotted in Fig. 1.

All metamaterials reported to date have consisted of elements repeated in cubic or other standard lattice configurations and are usually diagonal in the Cartesian basis. The layout of our cylindrical cloak, however, uses cells that are diagonal in a cylindrical basis and has "unit cells" that are curved sectors with varied electromagnetic environments. The correct retrieval procedure that would obtain the effective medium properties from such irregular unit cells is not yet available. Given that the curvature is not extreme in this cloak design, however, we modeled the unit cells as right-rectangular prisms in a periodic array of like cells, with the assumption that the actual cells will produce minor corrections in the effective medium properties.

Because of constraints of the layout, we chose a rectangular unit cell with dimensions $a_\theta = a_z$ = 10/3 mm and a_r = 10/π mm. We were able to obtain both the desired ε_z and $\mu_r(r)$ from an SRR by tuning two of its geometric parameters: the length of the split s and the radius of the corners r (Fig. 2). The parameters r and s shift the frequency of the electric and magnetic resonance, respectively, though there is some cross-coupling that must be compensated for.

Using commercial, full-wave, finite-element simulation software (Microwave Studio, Computer Simulation Technology), we performed a series of scattering (*S*) parameter simulations for the SRR unit cells over a discrete set of the parameters r and s covering the range of interest. A standard retrieval procedure (*18*, *19*) was then performed to obtain the effective material properties ε_z and μ_r from the *S* parameters. The discrete set of simulations and extractions was interpolated to obtain the particular values of the geometric parameters that yielded the desired material properties. We chose an operating frequency of 8.5 GHz, which yields a reasonable effective medium parameter $\lambda/a_\theta > 10$, where λ is the wavelength in free space.

The layout consisted of 10 concentric cylinders, each of which was three unit cells tall. The evenly spaced set of cylinder radii was chosen so that an integral number of unit cells fit exactly around the circumference of each cylinder, necessitating a particular ratio of radial-to-circumferential unit cell size. We chose to increase the number of unit cells in each successive cylinder by six, enabling us to use six supporting radial spokes that can intersect each of the cylinders in the spaces between the SRRs. This led to the requirement $a_r/a_\theta = 3/\pi$. Additionally, to minimize the magnetoelectric coupling inherent in single-split SRRs (*20*), we alternated their orientation along the z direction (Fig. 1).

The overall scale of the cloak is such that a complete field mapping of the cloak and its immediate environment is feasible (Fig. 3). By the same reasoning, numerical simulations of the cloak are also feasible, so long as the cloak is approximated by continuous materials. A complete simulation of the actual cloak structure, including the details of the thousands of SRRs, would be impractical for general optimization studies.

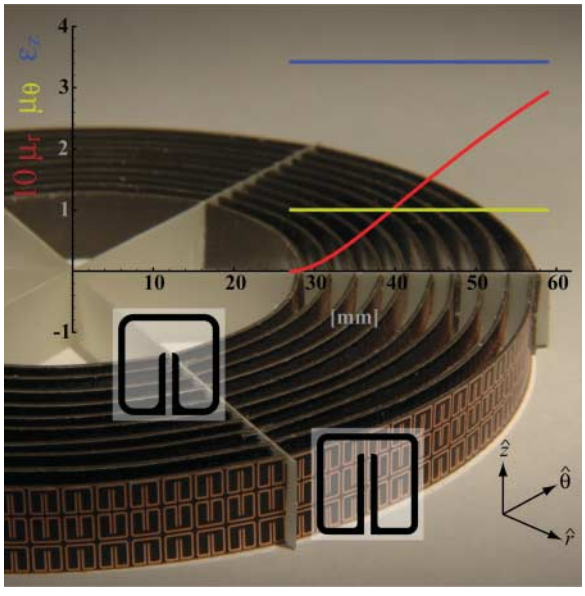

Fig. 1. 2D microwave cloaking structure (background image) with a plot of the material parameters that are implemented. μ_r (red line) is multiplied by a factor of 10 for clarity. μ_θ (green line) has the constant value 1. ε_z (blue line) has the constant value 3.423. The SRRs of cylinder 1 (inner) and cylinder 10 (outer) are shown in expanded schematic form (transparent square insets).

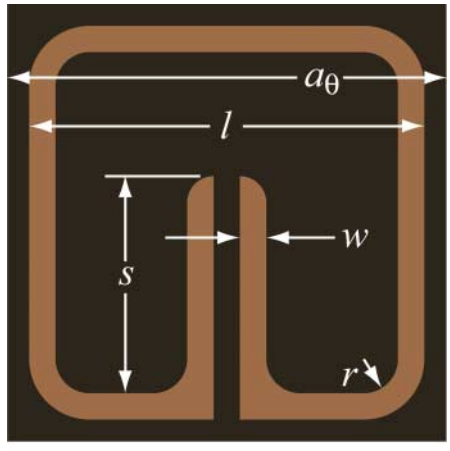

cyl.	r	s	μ_r
1	0.260	1.654	0.003
2	0.254	1.677	0.023
3	0.245	1.718	0.052
4	0.230	1.771	0.085
5	0.208	1.825	0.120
6	0.190	1.886	0.154
7	0.173	1.951	0.188
8	0.148	2.027	0.220
9	0.129	2.110	0.250
10	0.116	2.199	0.279

Fig. 2. SRR design. The in-plane lattice parameters are $a_\theta = a_z$ = 10/3 mm. The ring is square, with edge length l = 3 mm and trace width w = 0.2 mm. The substrate is 381-μm-thick Duroid 5870 (ε = 2.33, t_d = 0.0012 at 10 GHz, where t_d is the loss tangent). The Cu film, from which the SRRs are patterned, is 17 μm thick. The parameters r and s are given in the table together with the associated value of μ_r. The extractions gave roughly constant values for the imaginary parts of the material parameters, yielding 0.002 and 0.006 for the imaginary part of ε_z and μ_r, respectively. The inner cylinder (cyl.) is 1 and the outer cylinder is 10.

Continuous medium simulations of cloaking structures were performed by means of the COMSOL Multiphysics finite-element–based electromagnetics solver (*12*). The simulation result of the ideal case is shown in Fig. 4A, with material properties as in Eq. 2, and no absorption loss. Several real-world effects were incorporated into another simulation (Fig. 4B) to match experimental conditions as much as possible. In the latter simulation, the reduced material properties of Eq. 3 were used, and $\mu_r(r)$ was approximated by a 10-step piecewise constant function to mimic the concentric rings of the fabricated cloak. Additionally, absorption loss was added corresponding to that found in the unit cell simulations (and given in Fig. 2).

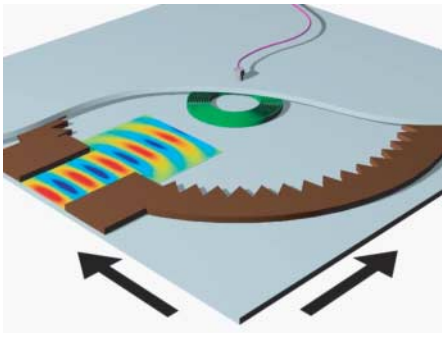

Fig. 3. Cutaway view of the planar waveguide apparatus. Microwaves (red and yellow patterns) are introduced by means of a coaxial-to-waveguide transition (not shown) attached to the lower plate (lined with a circular sawtooth-shaped microwave absorber). An antenna mounted in the fixed upper plate measures the phase and amplitude of the electric field. To perform field maps, we stepped the lower plate in the lateral directions (black arrows).

For the experimental confirmation, we measured the metamaterial cloak in a parallel-plate waveguide comprising two flat conducting (Al) plates spaced 11 mm apart (Fig. 3). Microwaves were introduced through an X-band (8 to 12 GHz) coax-to-waveguide adapter that was attached to the lower plate and were incident on the cloak, which rested on the lower plate and was nearly of the same height (10 mm) as the plate separation.

A field-sensing antenna was formed from a coaxial fixture inserted into a hole drilled through the upper plate. The center conductor and dielectric of the coaxial connector extended to a position flush with the lower surface of the upper plate and did not protrude into the chamber volume. The lower plate was mounted on two orthogonal linear translation stages, so that the lower plate (including the cloak, waveguide feed, and absorber) could be translated with respect to the upper plate and to the detector. By stepping the lower plate in small increments and recording the field amplitude and phase at every step, a full 2D spatial field map of the microwave scattering pattern could be acquired both inside the cloak and in the surrounding free-space region. Further experimental details can be found in (*16*) and in the supporting online material.

Both the cloak surrounding a 25-mm-radius Cu cylinder (Fig. 4D) and the bare Cu cylinder (Fig. 4C) were measured. The samples were placed on the lower plate in the center of the mapping region and illuminated with microwaves over a discrete set of frequencies that included the expected operating frequency of the cloak. At each frequency, the complex electric field was acquired, and the process was repeated for all x and y positions in the scan range. After reviewing the field maps at all frequencies, the optimal frequency for the cloak sample was determined to be 8.5 GHz, in near-exact agreement with the design target. The optimal frequency was selected as that which best matched the simulated field plots. The acquired real part of the electric field distribution is shown (Fig. 4, C and D).

Comparison of Fig. 4, C and D, shows that the cloak reduces both backscatter (reflection) and forward scatter (shadow). The backscatter is particularly evident in movie S3 as a strong standing-wave component. Comparison of Fig. 4, B and D, shows that the field plots found through full-wave simulations are in marked agreement with the experimental data. The underlying physics of the cloaking mechanism can be studied even further by viewing the field animations (movies S1 to S5). As the waves propagate through the cloak, the center section of the wavefront begins to lag as it approaches the inner radius, exhibiting a compression in wavelength and a reduction in intensity. The wavefront then separates to pass around the cloak hole and reforms on the opposite side, where its center section initially leads the wavefront. The wavefronts at the boundary of the cloak match the wavefronts outside the cloak, which essentially correspond to those of empty space. The scattering is thus minimized, though not perfectly, as a result of the reduced parameter implementation. The fields on the exit side are noticeably attenuated because of the absorption of the cloak material.

The agreement between the simulation and the experiment is evidence that metamaterials can indeed be designed to detailed and exacting specifications, including gradients and non-rectangular geometry. Though the invisibility is imperfect because of the approximations used and material absorption, our results do provide an experimental display of the electromagnetic cloaking mechanism and demonstrate the feasibility of implementing media specified by the transformation optics method with metamaterial technology.

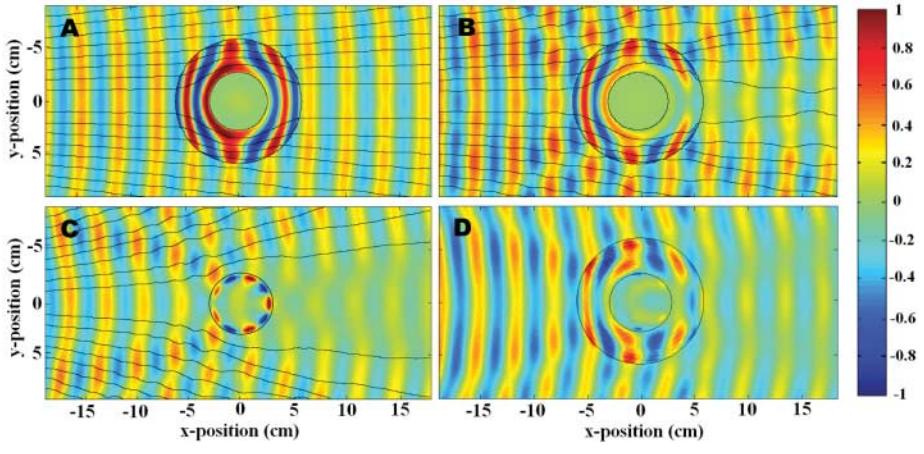

Fig. 4. Snapshots of time-dependent, steady-state electric field patterns, with stream lines [black lines in (A to C)] indicating the direction of power flow (i.e., the Poynting vector). The cloak lies in the annular region between the black circles and surrounds a conducting Cu cylinder at the inner radius. The fields shown are (**A**) the simulation of the cloak with the exact material properties, (**B**) the simulation of the cloak with the reduced material properties, (**C**) the experimental measurement of the bare conducting cylinder, and (**D**) the experimental measurement of the cloaked conducting cylinder. Animations of the simulations and the measurements (movies S1 to S5) show details of the field propagation characteristics within the cloak that cannot be inferred from these static frames. The right-hand scale indicates the instantaneous value of the field.

References and Notes

1. J. B. Pendry, D. Schurig, D. R. Smith, *Science* **312**, 1780 (2006).
2. U. Leonhardt, *Science* **312**, 1777 (2006).
3. A. J. Ward, J. B. Pendry, *J. Mod. Opt.* **43**, 773 (1996).
4. U. Leonhardt, T. G. Philbin, *N. J. Phys.* **8**, 247 (2006).
5. D. Schurig, J. B. Pendry, D. R. Smith, *Opt. Express* **14**, 9794 (2006).
6. A. Alu, N. Engheta, *Phys. Rev. E Stat. Nonlin. Soft Matter Phys.* **72**, 016623 (2005).
7. G. W. Milton, N.-A. P. Nicorovici, *Proc. R. Soc. London Ser. A* **462**, 1364 (2006).
8. A. I. Nachman, *Ann. Math.* **128**, 531 (1988).
9. G. Gbur, *Prog. Opt.* **45**, 273 (2003).
10. A. Greenleaf, M. Lassas, G. Uhlmann, *Physiol. Meas.* **24**, 413 (2003).
11. A. Greenleaf, M. Lassas, G. Uhlmann, *Math. Res. Lett.* **10**, 1 (2003).

12. S. A. Cummer *et al.*, *Phys. Rev. E* **74**, 036621 (2006).
13. D. R. Smith, J. B. Pendry, M. C. K. Wiltshire, *Science* **305**, 788 (2004).
14. R. B. Greegor *et al.*, *Appl. Phys. Lett.* **87**, 091114 (2005).
15. T. Driscoll *et al.*, *Appl. Phys. Lett.* **88**, 081101 (2006).
16. B. J. Justice *et al.*, *Opt. Express* **14**, 8694 (2006).
17. J. B. Pendry, A. J. Holden, D. J. Roberts, W. J. Stewart, *IEEE Trans. Micr. Theory Techniques* **47**, 2075 (1999).
18. D. R. Smith, S. Schultz, P. Markoš, C. M. Soukoulis, *Phys. Rev. B* **65**, 195104 (2002).
19. X. Chen, T. M. Grzegorczyk, B.-I. Wu, J. Pacheco, J. A. Kong, *Phys. Rev. E Stat. Nonlin. Soft Matter Phys.* **70**, 016608 (2004).
20. R. Marqués, F. Medina, R. Rafii-El-Idrissi, *Phys. Rev. B* **65**, 14440 (2002).
21. D.S. acknowledges support from the Intelligence Community Postdoctoral Research Fellowship program. L. Guo was instrumental in establishing our data acquisition and motion-control capabilities. J.B.P. thanks the Engineering and Physical Sciences Research Council for a Senior Fellowship.

Supporting Online Material
www.sciencemag.org/cgi/content/full/1133628/DC1
SOM Text
Figs. S1 to S3
Movies S1 to S5

8 August 2006; accepted 3 October 2006
Published online 19 October 2006;
10.1126/science.1133628
Include this information when citing this paper.

Isotopic Evidence for Dietary Variability in the Early Hominin *Paranthropus robustus*

Matt Sponheimer,[1] Benjamin H. Passey,[2] Darryl J. de Ruiter,[3] Debbie Guatelli-Steinberg,[4] Thure E. Cerling,[2,5] Julia A. Lee-Thorp[6]

Traditional methods of dietary reconstruction do not allow the investigation of dietary variability within the lifetimes of individual hominins. However, laser ablation stable isotope analysis reveals that the $\delta^{13}C$ values of *Paranthropus robustus* individuals often changed seasonally and interannually. These data suggest that *Paranthropus* was not a dietary specialist and that by about 1.8 million years ago, savanna-based foods such as grasses or sedges or animals eating these foods made up an important but highly variable part of its diet.

Both dental microwear texture analysis (*1*) and stable carbon isotope analysis (*2*–*5*) have demonstrated that the diets of South African australopiths were variable on the whole, but it has not been clear how the diets of individual hominins varied during their lifetimes. Here we provide evidence for short-term (seasonal and interannual) dietary change within the lifetimes of individual hominins, using a laser ablation method for stable isotope analysis (*6*). This method allows analysis along the growth axis of hominin teeth at submillimeter increments, making it possible to trace an individual's dietary history.

In tropical environments, virtually all trees, bushes, shrubs, and forbs use the C_3 photosynthetic pathway, whereas grasses and some sedges use the C_4 photosynthetic pathway (*7*, *8*). C_3 plants are depleted in ^{13}C [~ –27 per mil (‰)] as compared to C_4 plants (~ –12‰). The carbon isotopes in plants are incorporated into the tissues of consumers, with some additional fractionation (*9*, *10*), and consequently carbon isotope ratios of tooth enamel can reveal the degree to which an animal consumed C_3 or C_4 resources. This allows determination of whether a hominin ate C_3 foods, such as the forest fruits and leaves consumed by extant apes, or if they supplemented their diets with savanna-based C_4 foods, such as grasses or animals eating those plants (*2*).

We analyzed the enamel of four permanent teeth of *Paranthropus robustus* from Swartkrans, South Africa [found in member 1 at the site, dated ~1.8 million years ago (Ma)] using laser ablation stable isotope analysis (*11*). We also analyzed enamel of three contemporaneous browsing herbivores (*Raphicerus* sp.) from Swartkrans to control for postmortem alteration of carbon isotope ratios. We also counted the tooth growth increments (perikymata) that outcropped to the enamel surface between and adjacent to each ablation track on the hominin specimens to temporally constrain the isotope data where possible (Fig. 1). The number of days represented by perikymata is 9 days in humans and extant apes, with ranges from 6 to 12 days in humans and extant apes (*12*). Because the actual periodicities of perikymata in fossil teeth cannot be known without sectioning them, we assumed that the periodicity for *Paranthropus* was 7 days for this study (*12*).

The mean of all carbon isotopic analyses for *Raphicerus* demonstrates that diagenesis has not obliterated the biogenic carbon isotopic compositions, because it indicates a C_3 diet like that of *Raphicerus'* modern congeners (*13*) and of other known browsing herbivores from the site (Table 1 and table S1; $\delta^{18}O$ values are discussed in fig. S1) (*2*). Moreover, the expected small range in variation within individual *Raphicerus* teeth (a maximum of 0.9‰) shows that fossilization has not induced significant carbon isotopic variation at the spatial resolution of our analyses (Fig. 2). In contrast, there is strong variability within individual hominin teeth. The mean range of variation within individual teeth is 3.4‰ for *Paranthropus*, whereas the mean range for *Raphicerus* is only 0.7‰ ($P < 0.05$, Mann-Whitney *U* test, Table 1), showing that these hominins had more variable diets. In two out of four hominin teeth, the amplitude exceeds 4‰, which, at face value, suggests that their consumption of C_4 resources (tropical grasses or sedges or animals eating these foods) varied by ~40%. However, this isotopic signal is attenuated because of protracted mineral uptake during amelogenesis and our sampling protocol, which required some mixing of enamel layers (*14*).

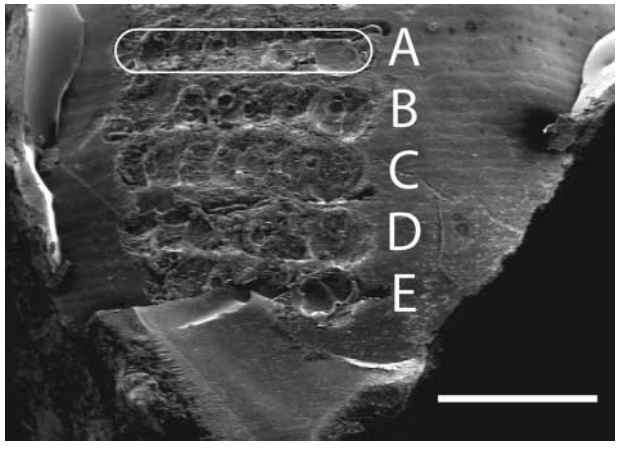

Fig. 1. A portion of the imbricational enamel of SKX 5939, on which the total number of perikymata between the first and last ablation samples shown (**A** to **E**) is 22, meaning that the interval represented by these samples is approximately 154 days (22 × 7). The day counts are only intended to be rough approximations sufficient to differentiate seasonal from interannual variability. The first visible ablation track is outlined in white. Perikymata are visible as faint horizontal lines across the tooth's surface. Scale bar, 1 mm.

[1]Department of Anthropology, University of Colorado at Boulder, Boulder, CO 80309, USA. [2]Department of Geology and Geophysics, University of Utah, Salt Lake City, UT 84112, USA. [3]Department of Anthropology, Texas A&M University, College Station, TX 77843, USA. [4]Department of Anthropology, The Ohio State University, Columbus, OH 43210, USA. [5]Department of Biology, University of Utah, Salt Lake City, UT 84112, USA. [6]Department of Archeological Sciences, University of Bradford, Bradford BD1 7DP, UK.